Published in final edited form as:
Sci Signal. ; 11(515): . doi:10.1126/scisignal.aaq1060.

KIF22 co-ordinates CAR and EGFR dynamics to promote cancer cell proliferation

Rosemary Pike[1], **Elena Ortiz-Zapater**[1,2], **Brooke Lumicisi**[1], **George Santis**[2], and **Maddy Parsons**[1,3]

[1]Randall Division of Cell and Molecular Biophysics, King's College London, New Hunt's House, Guys Campus, London, UK, SE1 1UL

[2]Division of Asthma, Allergy & Lung Biology, King's College London, 5th Floor Tower Wing, Guy's Hospital Campus, London, UK, SE1 1UL

Abstract

The Coxsackie and Adenovirus Receptor (CAR) is a transmembrane receptor that plays a key role in cell-cell adhesion. CAR is found in normal epithelial cells and is increased in abundance in various human tumors, including lung carcinomas. Here, we investigated the potential mechanisms by which CAR contributes to cancer cell growth and found that depletion of CAR in human lung cancer cells reduced anchorage-independent growth, epidermal growth factor (EGF)–dependent proliferation, and tumor growth in vivo. EGF induced the phosphorylation of CAR and its subsequent relocalization to cell junctions through the activation of the kinase PKCδ. EGF promoted the binding of CAR to the chromokinesin KIF22. KIF22-dependent regulation of microtubule dynamics led to delayed EGFR internalization, enhanced EGFR signaling, and coordination of CAR dynamics at cell-cell junctions. These data suggest a role for KIF22 in the coordination of membrane receptors and provide potential new therapeutic strategies to combat lung tumor growth.

Introduction

Coxsackie and Adenovirus (Ad) Receptor (CAR) was initially identified as the primary docking receptor for Coxsackie B viruses and members of the Ad family (1). Further work has since demonstrated that CAR and is an important cell adhesion molecule (2, 3) as a member of the Junction Adhesion Molecule (JAM) family that forms homo-dimers across cell-cell junctions (4, 5). We have previously shown that CAR is phosphorylated at Thr^{290} and Ser^{293} within the cytoplasmic domain by PKCδ and this controls E-Cadherin stability at adherens junctions (6, 7). Its role in cancer may be tissue-specific; the expression of the gene that encodes CAR is upregulated in some cancers and downregulated in others (8). In the lung however, CAR abundance is consistently increased in tumor tissue compared to normal

[3]To whom correspondence should be addressed: maddy.parsons@kcl.ac.uk.

Author contributions: MP and GS conceived the project. All authors contributed to experimental design and had intellectual input into the project planning. RP conducted experiments and analyzed data with help from BL. EO-Z conducted the xenograft studies and tissue analysis. MP wrote the manuscript with input from all other authors.

Competing interests: The authors all declare that they have no competing interests.

Europe PMC Funders Author Manuscripts

tissue, and reducing its expression in lung cancer cells reduces the growth of xenografts in animal models (9). Increased CAR abundance in lung cancer is associated with a more mesenchymal cell phenotype and increased expression of several mesenchymal markers (9). Other studies have shown that CAR promotes cell-cell adhesion and facilitates cell survival (10) and that transforming growth factor β (TGFβ)-induced epithelial-to-mesenchymal transition (EMT) is coupled with the downregulation of CAR (11) potentially leading to enhanced metastasis in vivo (12). In vitro, CAR depletion reduces the growth of lung cancer cells in soft agar, suggesting an important role in anchorage-independent growth (13). CAR may play a role in lung cancer cell adhesion and invasion (8) as well as being a potential marker of cancer stem cells in non-small cell lung cancers (NSCLC) that are resistant to paclitaxel and radiation treatment (14). Despite this growing evidence that implicates CAR in lung tumor progression, its mechanisms of action in this context is not clear.

Growth factor signaling is an important driver of tumor growth, and mutations in growth factor receptors and downstream signaling molecules are frequently found in lung cancers (15). Gain-of-function mutations in the epidermal growth factor receptor (EGFR) are particularly prominent and well characterized in adenocarcinomas and provide a proliferative advantage (16). EGFR acts a node for a number of complex signaling networks and controls many cellular processes as well as proliferation, including DNA replication, adhesion and migration (17). In addition to the well-characterized role as a mitogen, EGFR also signals both upstream and downstream of cell-cell adhesion molecules (18). For example, cytokines are able to induce the disassembly of tight junctions in lung epithelial cells by activating EGFR and mitogen-activated protein kinase (MAPK) signaling (19). EGFR is also able to drive the phosphorylation of the polarity protein Par3 at tight junctions to determine the rate of tight junction assembly (20). Similarly, EGFR activity acts to regulate transcription of claudin and, in turn, positively regulates transepithelial resistance (21). E-cadherin promotes the activation of EGFR and MAPK signaling directly, suggesting that adhesion molecules regulate receptor tyrosine kinase (RTK) signaling (18). The loss of E-Cadherin during EMT can also activate MAPK signaling and invasive behavior specifically in NSCLC cells (22). This highlights the importance of cross talk between EGFR signaling and cell adhesion complexes in the regulation of tumor growth.

The cytoskeleton plays a key role in regulating cell adhesion and proliferation. CAR and EGFR require F-actin and/or microtubule cytoskeletons for membrane localization, signaling and trafficking (23, 24) and both localize to cell-cell contacts and play a role in controlling epithelial cell junction stability (6, 7, 25). Here, we aimed to determine whether co-operation exists between these two receptors and found that CAR and EGFR act in concert to co-ordinate and enhance cancer cell proliferation. Our data demonstrates a role for CAR in controlling EGFR signaling through a direct interaction with the chromokinesin KIF22. We show that CAR promotes tumor cell proliferation downstream of EGFR both in vivo and in vitro. We further show that EGFR indirectly phosphorylates CAR that in turn provides junctional adhesion maintenance in EGF-stimulated cells through relocation at cell contact sites. Moreover, we show that this relocation relies upon an EGF-induced CAR-KIF22 complex. Our data reveal a new interplay between two key receptors known to be dysregulated in tumors and provide potential new avenues for therapeutic targeting of solid tumor growth.

Results

CAR mediates EGF-dependent lung cancer cell proliferation

A previous study has shown that antisense mediated depletion of CAR in NCI-H1703 NSCLC cells resulted in reduced proliferation (13). To determine whether depletion of CAR in other human lung cancer cells alters proliferation, we used shRNA to stably deplete CAR from A549 and H1975 cells (Fig 1A, Supp Fig 1A). Proliferation was monitored over 48 hours in the presence or absence of serum as growth stimulants. Resulting analysis demonstrated that depletion of CAR significantly reduced proliferation in both cells lines (Fig. 1B, fig. S1B). Given that normal lung epithelial cells also express CAR, we also determined whether CAR could control proliferation in this context. We depleted or overexpressed CAR in the human lung epithelial line 16HBE using two targeted short hairpin RNAs (shRNAs) and a green fluorescent protein (GFP)-tagged wild-type CAR construct, respectively (7, 26) and analyzed cell proliferation over 48 hours. CAR knockdown significantly reduced, whereas CAR overexpression significantly increased, proliferation in 16HBE cells (fig. S1C) confirming that CAR plays a key role in this process in both normal epithelial cells as well as epithelial-derived carcinoma cells. Because EGF is known to play a key role in proliferation of lung cancer cells in vivo, we next tested whether CAR contributed to EGF-specific proliferation in these cells. CAR depletion significantly reduced proliferation in both A549 and H1975 cells treated with EGF (Fig. 1B, fig. S1D). However, knocking down CAR had no effect on cell proliferation induced by hepatocyte growth factor (HGF; fig. S1E, suggesting that CAR plays a role in EGF-but not other ligand-dependent signals that promote cell growth.

Soft agar colony assays revealed that CAR knockdown markedly reduced anchorage-independent growth in both A549 and H1975 cells (Fig. 1C and fig. S1F). To further determine whether the in vitro defects in proliferation seen in CAR-depleted cells also translated to in vivo settings, we performed subcutaneous injections of matched control or CAR-depleted H1975 cells into the flanks of immunocompromised mice. Analysis of tumor growth over time revealed a significant defect in tumor growth in CAR-depleted cells, resulting in smaller tumors at the time of sacrifice (Fig. 1D). To confirm that this reduced tumor size was due to reduced cell proliferation, sections of fixed tumors were stained for both phosphorylated Histone H3 and Ki-67 (Fig. 1E). Quantification demonstrated a significant reduction in both markers in CAR-depleted tumors (Fig 1F). Therefore, these data demonstrate that CAR promotes proliferation of human lung cancer cells both in vitro and in vivo.

CAR promotes post-mitotic daughter cell attachment and spreading

To determine the nature of the defect in CAR-knockdown cells that leads to reduced proliferation, we performed time-lapse imaging of control or CAR-depleted A549 cells under growth-inducing conditions. Analysis of resultant movies demonstrated that CAR-knockdown cells were significantly slower to re-spread after division (Fig. 2, A and B), and junctions between daughter cells were more transient than in control cells resulting in a greater proportion of cells undergoing complete separation post-division (Fig. 2B). This suggested that CAR plays a role in coordinating and maintaining contacts between adjacent

daughter cells, as well as other neighboring cells within colonies, potentially to support efficient re-spreading and growth signaling. To determine localization of CAR during mitosis, we further analyzed movies of A549 cells co-expressing CAR-GFP and Histone H2B type 1-K (H2BK)-mCherry to mark the nuclei during division. These movies revealed that CAR was rapidly recruited to newly forming contacts between daughter cells after division, further supporting the notion that CAR may play a key role in stabilizing these adhesions (Fig. 2C).

EGF promotes CAR phosphorylation and relocalization at cell-cell adhesions

Given that our data demonstrated that CAR played a key role in EGF-dependent proliferation, we next sought to further investigate the potential mechanisms governing this response. We first analyzed whether CAR plays a role in regulating EGFR activation or signaling upon ligand binding. There was no difference in the phosphorylation of EGFR or the activation of the key downstream signaling molecule extracellular signal-regulated kinase (ERK) 1 and ERK2 in control or CAR-knockdown A549 cells (fig. S2A). In agreement with this, phospho-EGFR levels were also unchanged in tissue samples of CAR-knockdown A549 xenografts compared to controls (fig. S2B). Moreover, neither phospho-ERK levels nor degradation of EGFR over longer time courses upon high concentrations of EGF stimulation (100 ng/ml) were altered by CAR depletion (fig. S2C). We therefore hypothesized that EGFR may be acting upstream of CAR in controlling proliferation. To better define the relationship between CAR and EGFR, we performed live cell confocal time-lapse imaging of CAR-GFP expressed in A549 cells after stimulation with EGF. Analysis of resultant movies demonstrated that CAR moved from the periphery of junctions between cells towards the center in response to EGF (Fig. 3A). The same CAR redistribution was also seen in images of cells fixed following EGF stimulation and stained for endogenous CAR and EGFR (fig. S2D). Analysis of CAR and EGFR in these images also demonstrated a high degree of colocalization between the two receptors at cell-cell adhesion sites, which was significantly reduced after 15 and 60 min of EGF stimulation and EGFR internalization, further demonstrating that CAR is retained at adhesion sites after EGFR endocytosis (fig. S2D).

Our previous studies have shown that phosphorylation of the CAR cytoplasmic tail at Thr^{290}/Ser^{293} can regulate dynamics of CAR at epithelial cell junctions (7, 26). To determine whether EGF may act through phosphorylation of CAR to elicit junctional movement, we analyzed the levels of Thr^{290}/Ser^{293} phosphorylated CAR (p-CAR) in EGF-stimulated A549 cells. Western blotting revealed a significant increase in the amount of p-CAR after 15 min of EGF stimulation that was maintained up to 60 min after (Fig. 3B) and this increase was also observed by immunostaining for p-CAR in fixed cells (Fig. 3C). We further demonstrated that depletion of protein kinase C δ (PKCδ), the kinase that phosphorylates these sites in CAR (7), inhibited EGF-induced phosphorylation of CAR, suggesting that EGFR-dependent PKCδ activation may contribute to CAR dynamics (Fig. 3D). To test this concept further, we expressed a non-phosphorylatable mutant of CAR (AA-CAR) (26) in A549 cells and analyzed CAR redistribution after stimulation with EGF in A549 cells by live confocal time-lapse imaging. AA-CAR-GFP did not undergo translocation within cell junctions in response to EGF as compared to wild-type CAR-GFP

(Fig. 3, A and E). These data together demonstrate that EGF stimulation can promote phosphorylation of CAR and that this in turn acts to promote translocation of CAR within cell-cell junctions.

CAR binds to KIF22

Our data thus far shows that CAR can move laterally within the junction in an EGF and phosphorylation-dependent manner, but we had yet to determine the molecular mechanisms that may mediate this dynamic repositioning. To identify potential binding partners for CAR involved in this process, we performed analyzed the proteins that associated with the CAR cytoplasmic tail in pulldowns from A549 cell lysates. Silver staining and mass spectrometry analysis of CAR-bound complexes subsequently revealed that multiple peptides mapping to the chromokinesin KIF22 (also known as KID) pulled down with the wild-type but not AA-mutant CAR cytoplasmic tail (fig. S3A). This interaction was subsequently validated in pulldown assays using GST-CAR cyto domain protein (Fig. 4A) and through immunoprecipitation of CAR followed by probing with antibodies specific to KIF22 (Fig. 4B). Compared to wild-type CAR, AA-CAR-GFP showed significantly lower binding to KIF22 (Fig. 4B), suggesting phosphorylation of CAR promotes formation of this complex. Moreover, we observed an increase in CAR-KIF22 binding by co-immunoprecipitation (co-IP) in cells treated with EGF, suggesting a potential role for this complex in mediating CAR-dependent responses to EGF (Fig 4C). Pre-incubation of these cells with the EGFR tyrosine kinase inhibitor AG1478 prior to immunoprecipitation led to a significant reduction in both CAR-associated KIF22 and levels of p-CAR (Fig. 4C), further suggesting that EGFR activation is required for formation of the KIF22 via CAR phosphorylation. To better define the binding region(s) within KIF22 for CAR, we expressed a series of FLAG-tagged truncation mutants of KIF22 (Fig 4D) (27) in HEK293 cells and performed pulldowns from lysates using the GST-CAR cytoplasmic domain. The resulting blots confirmed binding to full-length KIF22 (FL-KIF22) and additionally demonstrated specific binding to mutant constructs (called D1 and D2) that contain N-terminal motor domains (MD) but lack the DNA binding domain (DBD) (Fig 4D). This suggests that the CAR-binding interface within KIF22 lies within its N-terminal region. Moreover, binding to CAR was greater for the KIF22-D1 mutant construct (which also lacks the coiled coil-domain; CCD) than for either full-length KIF22 or the -KIF22-D2 mutant, suggesting that the presence of the CCD may act to limit binding to CAR.

The CCD region in other kinesin family members, such as kinesin-1 and kinesin-5 have previously been shown to regulate dimerization and cargo binding (28) but the potential for this region to regulate KIF22 self-association remains unclear. To test whether KIF22 may self-associate, we performed in vitro GST pulldown assays using purified GST-tagged N-terminal or C-terminal domain constructs of KIF22 (GST-NT-KIF22 and GST-CT-KIF22; Fig. 4E) co-incubated with a purified FLAG-tagged full-length KIF22 construct (FLAG-KIF22-FL). The C-terminal containing the CCD, but not the N-terminal, of KIF22 associated with the full-length construct, supporting the notion that the CCD may mediate self-binding (Fig. 4E). To test this directly, we performed GST pulldowns using GST-CT-KIF22 incubated with FL-KIF22 protein in the presence or absence of recombinant purified CCD-HALO. Data demonstrated a significant reduction in binding between the C-terminal

and full-length constructs in the presence of excess CCD (Fig. 4F), suggesting that the CCD of KIF22 acts to maintain self-binding. Moreover, expression of CCD-HALO in A549 cells led to a relocalization of endogenous KIF22 from the nucleus to the cytoplasm (fig. S3B), suggesting that interfering with the potentially dimeric self-association of KIF22 can promote cytoplasmic localization of this protein. Together, this data demonstrates that KIF22 is able to bind to itself to potentially form dimers via the CCD and that preventing this interaction can induce its cytoplasmic localization.

KIF22 regulates EGFR signaling and internalization

KIF22 has previously been shown to positively regulate proliferation through control of chromosome separation (29–31), but its potential roles in the cytoplasm during interphase is not known. Because our data thus far showed that KIF22 forms a complex with CAR and potentially localizes to the cytoplasm of cells during interphase, we explored the potential role of KIF22 in mediating CAR-dependent, EGF-induced proliferation. We first sought to confirm previous studies showing a role for KIF22 in controlling proliferation. To this end, we depleted KIF22 from A549 cells using two specific siRNAs (fig. S4A) and analyzed proliferation under normal culture conditions using both fixed and live imaging approaches. Both methods demonstrated a significant reduction in proliferation in KIF22-knockdown cells (fig. S4, B and C). We further analyzed responses of these cells specifically in response to stimulation with EGF. KIF22 knockdown significantly reduced EGF-dependent proliferation (Fig. 5A) and ERK activation in A549 cells (Fig. 5B), suggesting that EGFR responses to ligand are mediated by KIF22.

EGFR undergoes dimerization at the plasma membrane in response to ligand binding and this results in recruitment of adaptor proteins that are essential to initiate downstream signaling. This then leads to EGFR endocytosis resulting in termination of signaling and either receptor recycling or degradation (32, 33). However, because a number of reports have also shown that EGFR internalization can sustain signaling in certain cell types (34, 35), we sought to determine the extent to which EGFR endocytosis contributes to signaling in A549 cells. Cells pre-incubated with Dynasore (to block dynamin-dependent endocytosis) or nocodazole (to depolymerise microtubules and prevent post-endocytic transport) were treated with EGF and lysates analyzed by Western blotting. There was no significant change in EGF-dependent p-EGFR or p-ERK levels in either case (fig. S5), suggesting that endocytosis does not substantially contribute to the magnitude of receptor activation or p-ERK signaling in these cells.

To investigate whether KIF22 may regulate EGFR retention at the plasma membrane and thus promote signaling, we performed surface biotinylation assays in control or KIF22-knockdown A549 cells. Biotinylation of all plasma membrane proteins was performed, followed by EGF stimulation at different time points to induce surface EGFR internalization. A mild acid strip was then performed to remove any remaining surface biotin, followed by cell lysis and Streptavidin immunoprecipitation to isolate only the internalized pool of biotinylated EGFR. Analysis of internalization kinetics revealed no change in surface EGFR levels under serum-starved conditions but a significant increase in EGFR internalization 15 min after the addition of EGF when KIF22 was knocked down (Fig 5C). Re-probing these

blots revealed that no internalization of CAR occurred over the same time frame (Fig 5C), in agreement with confocal images of CAR and EGFR in control cells (fig. S2C). We further confirmed this rapid internalization of EGFR in KIF22-knockdown cells treated with EGF by immunostaining for and quantifying junction-associated EGFR over time (Fig 5D).

Because our data indicated that KIF22 regulates EGFR signaling and that CAR is relocalized upon EGF stimulation, we investigated whether KIF22 also played a role in CAR localization within junctions. Live imaging and analysis demonstrated that CAR-GFP in KIF22-depleted cells was localized across the entire junction and did not undergo relocalizion in response to EGF (Fig 6A), similar to that seen in cells expressing AACAR-GFP (Fig 3E). To further define the KIF22-dependent co-ordination of EGF-induced CAR and EGFR movement within junctions, we performed live imaging of A549 cells co-expressing CAR-GFP and EGFR-mCherry transfected with control or KIF22 siRNA. Resulting images (Fig 6B) and subsequent intensity analysis of signal at junctions (Fig 6C) demonstrated that the abundance of CAR within the central region of the junction increased after ~10 mins of EGF stimulation, and this was rapidly followed by a reduction of EGFR at the membrane (Fig 6B, left panels; and Fig 6C, left graph). Conversely, KIF22-depleted cells showed very little change in CAR abundance within the junction over the 30-min time course, but a rapid induction of EGFR internalization from the membrane (~2-4 mins) was seen in response to EGF, further supporting the notion that KIF22 can stabilize EGFR at the plasma membrane. Together, these findings demonstrate a role for KIF22 in controlling both movement of CAR within junctions and more controlled, slower internalization kinetics of EGFR from the plasma membrane. This further suggests that by acting upstream of both receptors, KIF22 is playing a key role in controlling the initiation of EGF-dependent proliferative responses in lung cancer cells.

KIF22 regulates peripheral microtuble stability in cells in interphase

As KIF22 is known to bind to microtubules, and microtubules are known to be important in receptor traffic, including EGFR (24, 36), we next sought to determine whether KIF22 could regulate EGFR through control of cytoskeletal dynamics in cells in interphase. To analyze the potential effects of KIF22 on the microtubule network architecture, we first stained fixed control or KIF22-knockdown cells for tubulin and F-actin. Images and subsequent quantification revealed that KIF22-depleted cells exhibit a more spread, peripherally-extended microtubule network (Fig 7A). To further define whether this defect might be due to altered microtubule dynamics, we imaged GFP-tubulin expressed in control or KIF22-knockdown A549 cells using live cell time-lapse confocal microscopy for up to 60 min after the application of EGF. Analysis of resulting movies demonstrated that treatment of control cells with EGF resulted in more stable microtubules that showed a reduction in growth rate coupled with significantly longer time periods in the growth phase and reduced catastrophe events (Fig. 7, B and C). Conversely, KIF22-knockdown cells showed constitutively more stable microtubules under basal conditions compared to control cells and tubulin dynamics were unchanged in the presence of EGF (Fig. 7, B and C). Moreover, levels of acetylated tubulin, that is associated with a more stable microtubule network, were also increased in KIF22-knockdown cells, further suggesting that KIF22 may enhance microtubule dynamics (Fig 7D). These findings support the notion that KIF22 can regulate the stability and

organization of the microtubule cytoskeleton in cells in interphase and this in turn may impact on receptor traffic and movement at the plasma membrane.

Cytoplasmic KIF22 coordinates EGFR signaling

Thus far, our data has demonstrated that KIF22 can self-associate via the CCD (Fig. 4, E and F) and that this may occlude the KIF22-CAR binding site within the N-terminus (Fig. 4D) and regulate subcellular localization of KIF22 (fig. S3B). We therefore hypothesized that the N-terminus of KIF22 may be sufficient to regulate EGFR membrane retention and signaling in response to EGF binding. To investigate this possibility, we depleted KIF22 from A549 cells and re-expressed either FLAG-KIF22-D3 (in which the N-terminus lacks the CCD and DBD) or FLAG-KIF22-D5 (in which the C-terminus lacks the MTD) (Fig 8A) and quantified EGFR abundance at the plasma membrane after 15 min of EGF stimulation. Analysis of confocal images demonstrated clear retention of EGFR at the plasma membrane of cells re-expressing KIF22-D3 but not KIF22-D5 compared to the KIF22-depleted cells within the same field of view (Fig. 8, A and B). Moreover, closer inspection of the localization of KIF22-D3 revealed cytoplasmic microtubule-like association of this mutant and a proportion of plasma membrane associated KIF22 that showed overlap with EGFR at this location (Fig. 8C). Staining of parallel coverslips or western blotting of lysates with antibodies to p-EGFR further demonstrated the KIF22-D3–associated, plasma membrane-localized EGFR was phosphorylated (Fig. 8, D and E), suggesting that cytoplasmic KIF22 is important for sustained EGFR signaling in response to ligand. Our previous data suggested that KIF22 acts upstream of both EGFR and CAR in controlling proliferation. To further confirm this relationship, we performed double knockdown of CAR and KIF22 in A549 cells and analyzed EGFR retention at the membrane in cells re-expressing KIF22-D3. Resulting quantification showed KIF22-D3 was able to restore membrane-associated EGFR in CAR-depleted cells (Fig. 8E), confirming that KIF22 acts on both EGFR and CAR to ultimately promote efficient cell division.

Discussion

The precise co-ordination of growth factor and adhesion receptors is essential to facilitate cancer cell division in solid tumors. Data presented in this study reveals a novel requirement for co-operation between two key plasma membrane receptors, CAR and EGFR in controlling proliferation in tumor cells. We additionally demonstrate a novel role for the chromokinesin KIF22 in co-ordinating these receptors. Our data supports a model whereby KIF22 can act in interphase to regulate microtubule stability and promote EGFR signaling that in turn regulates positioning of CAR at the plasma membrane to support efficient progression to cell division (Fig 8F). Potential functions for KIF22 outside of chromosome movement are poorly studied and our data provides new insight into previously unexplored roles for KIF22 within the cytoplasm in interphase.

A recent study showed the putative *Drosophila* homologue of KIF22 (KLP68D) is involved in synaptic development and neuromuscular junctions (37). Moreover, the same family of Kinesins has been implicated in transporting junctional proteins such as E-Cadherin as cargo to facilitate adherens junction formation in *Drosophila* photoreceptors (38). A large-scale

mass spectrometry screen recently identified the junctional protein MUPP1 as a putative interaction partner of KIF22, although this interaction has yet to be validated (39). A number of other non-nuclear proteins were also identified as potential interaction partners in this screen, including the adhesion scaffold protein PINCH and EPB41L4B, a regulator of RhoA GTPase activity. This supports our findings and further suggests that KIF22 may form additional interactions outside of the nucleus to control adhesion stability and cytoskeletal dynamics.

KIF22 depletion led to re-organization of CAR at cell-cell adhesion sites to a more stable, tightly defined contact site. Microtubules can target tight and adherens junctions to regulate dynamics (40, 41) therefore KIF22 may regulate CAR localization by bridging CAR and the microtubule network to allow junctional re-positioning. Mechanical forces are known to influence cell-cell adhesion protein dynamics and it is plausible that the change in CAR localization may also be as a result of local tension changes at the junction (42). Moreover, sub-membranous microtubules can disrupt the actomyosin network, which can increase the diffusion of receptors through membrane regions where actin resistance is low (43). Future studies aimed at understanding how cytoskeletal-dependent mechanical forces at cell-cell adhesion sites influence CAR homodimerization, and how this is regulated by KIF22, will be important to provide further insight into this process.

CAR has two potential binding sites within KIF22: one at the N-terminal region of the protein and the second within the region between the primary motor domain and the CCD. Similar regions in KIF22 are also required for interactions with the checkpoint protein CHFR (27), suggesting that KIF22 may adopt a certain conformation that exposes these specific sites to promote binding. KIF22 has previously been reported to be a monomer and that the putative CCD is shorter than conventional kinesins that dimerize (Shiroguchi et al., 2003). Our data and that from mass spec analysis (39) contradict this notion and rather suggest that KIF22 can self-associate. Indeed, a number of other kinesins have been reported to adopt a conformation to induce auto-inhibition and prevent microtubule binding (44). Binding data between KIF22 and CAR shown here supports this theory, as the C-terminal binding site of CAR is obstructed when the CCD is present, and the CCD can compete self-association of KIF22. It has also been suggested that the CCD modulates the polar ejection force generated by KIF22 and this in turn prevents re-congression of chromosomes during anaphase (45). This provides further evidence that CCD is a key regulatory domain within KIF22, affecting its function and potential binding partners.

KIF22 binds to the C-terminus of CAR and that CAR phosphorylation at Thr^{290}/Ser^{293} occurs in an EGF and PKCδ-dependent manner, increasing the affinity of KIF22 for the cytoplasmic tail of CAR. EGF stimulation may also promote transient translocation of KIF22 to the plasma membrane to facilitate this interaction. However, KIF22 is required in the nucleus during mitosis, suggesting that EGF stimulation may promote KIF22-CAR complex formation to facilitate CAR relocalization in the short term, following which KIF22 is then shuttled to the nucleus where it acts on chromosome movement. KIF22 is also spatially regulated during the cell cycle through phosphorylation by CDK1 (46) and it is plausible that this may also regulate KIF22 localization into and out of the nucleus. Our data further shows that depletion of KIF22 from lung cancer cells decreases EGFR

phosphorylation and signaling, increases the rate of EGFR internalization leading to a marked reduction in EGF-dependent proliferation. Other kinesins have been implicated in later stages of EGFR trafficking, for example KIF16B modulates the recycling and degradation of EGFR through early endosome regulation (47). Nothing is currently known about potential roles for specific kinesin family members in very early stages of EGFR endocytosis. EGFR becomes dephosphorylated by protein tyrosine phosphatases when internalized (32). Therefore, an increase in the rate of internalization also increases the rate at which EGFR is dephosphorylated, supported by our demonstration of enhanced membrane associated EGFR phosphorylation in cells expressing non-nuclear targeted KIF22. EGFR retention at the plasma membrane is important for the assembly of EGFR signaling complexes, including initiation of MAPK and PI-3-K pathways (33). These pathways are key for promoting cell proliferation and accelerated internalization of EGFR into endosomes reduces signaling through these pathways. EGFR internalization is widely considered to act as a stop signal for EGFR signaling; however, EGFR has also been reported to retain some activity at endosomes in some cell types (48). Our data suggests that endocytosis does not significantly contribute to EGFR activation or downstream signaling to ERK in A549 cells, suggesting these cells rely on plasma membrane-associated EGFR for initiating and sustaining signaling after EGF binding. Further analysis will be required to determine the precise mechanism by which KIF22 acts on EGFR to retain signaling activity at the plasma membrane and whether phosphorylation downstream of specific extracellular cues act to control the subcellular distribution of KIF22.

Our data indicates KIF22 may have a novel role in microtubule polymerization in cells in interphase. Our analysis of microtubules in both fixed and live cells (Fig. 5) demonstrated that loss of KIF22 leads to a more spread microtubule network and higher growth rates and reduced dynamic instability in live cells. We also demonstrate that KIF22 depleted cells show higher levels of acetylated tubulin again indicating increased stability of the network. These three distinct sets of data combined strongly support our conclusions that loss of KIF22 leads to a net increase in microtubule growth resulting in expansion of the microtubule network towards the plasma membrane. We propose that this expanded microtubule network promotes EGFR internalization, and this notion is supported by our data showing that cytoplasmic, but not nuclear KIF22, can enhance levels of EGFR at the plasma membrane in KIF22-depleted cells (Fig. 8). Other characterized kinesins that function as depolymerases include the kinesin-8 family. This family of kinesins also have two microtubule binding sites with the second site is located at the C-terminus of the protein (49, 50). Therefore, the putative second microtubule binding site of KIF22 identified may be aiding depolymerase activity of KIF22 identified in this chapter (Shiroguchi et al., 2003). Increasing evidence suggests the importance of microtubule stability on EGFR internalization. It has been shown that microtubules facilitate the diffusion of EGFR clusters at the plasma membrane (51). Microtubule stabilisation by acetylation in EGFR endocytosis is also controlled through activity of the tubulin deacetylase HDAC6 that negatively regulates EGFR endocytosis through modulation of microtubule stability and transport of the receptor along microtubules (24). Moreover, microtubule targeting drugs that disrupt the tubulin network decrease phosphorylation of EGFR and downstream signaling in esophageal cancer (52). It has been proposed that blocking the addition of tubulin subunits can increase

catastrophe, by enabling GTP hydrolysis to reach the plus-end of the microtubules (53). Within 5 minutes of EGFR activation microtubules are stabilized, possibly in preparation for EGFR internalization and trafficking. Longer-term EGFR signaling drives an increase in KIF22 expression, and this may be a feedback loop to rectify the microtubule network through the depolymerase activity of KIF22.

In summary, we have shown that KIF22 is an important, previously unreported regulator of both EGFR and CAR dynamics in human cancer cells. We postulate that these three molecules act in concert to control efficient EGF-dependent proliferation in lung cancer cells that may ultimately promote CAR- and EGFR-dependent tumorigenesis. Future experiments will be aimed at understanding the mechanisms and spatiotemporal events controlling assembly of the CAR-KIF22 complex with a view to using blockade of this complex as a potential route for new therapeutic intervention in solid lung tumors.

Materials and Methods

Antibodies and reagents

Anti-CAR (H300), anti-HSC70 and anti-PKCδ antibodies were from Santa Cruz Technology. p-CAR Thr^{290}/Ser^{293} polyclonal antibody was previously described (7) and was developed by Perbioscience (Thermofisher) using the peptide Ac-RTS(pT)AR(pS)YIGSNH-C and was affinity purified before use. Anti-β-tubulin, anti-acetylated tubulin and anti-FLAG antibodies were from Sigma Aldrich. Anti-phospho-EGFR (Y1173), anti-phospho-ERK (T202/Y204), anti-EGFR and anti-ERK antibodies were from Cell Signalling. Anti-KIF22 antibody was from Genetex, anti-GAPDH was from Chemicon. Anti-GFP antibodies were from Roche (immunoblotting) and MBL (immunoprecipitation). Anti-Ki67 and anti-phospho H3 antibodies were from Leica. Anti-Halo-tag antibody and HaloTag™ direct ligand were from Promega. Anti-mouse HRP and anti-rabbit-HRP were from DAKO. Anti-mouse-568, anti-rabbit-568 and phalloidin-647 were all obtained from Invitrogen. Recombinant human EGF was acquired from Peprotech and CalyculinA, sodium orthovanadate and protease inhibitor cocktail 1 were obtained from Calbiochem. Nocodazole and Dynasore were from Sigma. KIF22 targeted siRNA were from Origene and CAR and non-targeting siRNA were acquired from Dharmacon. PKCδ targeting siRNA were from Ambion.

Plasmids

Full length and mutant CAR sequences were cloned in frame into pHR9SIN-SEW lentiviral expression vector, which was a gift from Prof Adrian Thrasher (Institute of Child Health, UCL) and into pGEX-2T. Phospho-mutant CAR constructs were generated using site directed mutagenesis and have been described previously (7). Control and CAR KD shRNA vectors (shA and shB) were in pLKO.1 backbones purchased from Sigma Mission collection (clone ID NM_001338). H2BK-GFP and mCherry plasmids and β-tubulin-GFP were kindly gifted from Dr James Monypenny (King's College London, UK). FLAG-tagged KIF22 constructs were a gift from Dr Maddika (CDFD; (27)). The cDNAs encoding the GST NT and CT KIF22 domains, were kindly provided by Andy Wilde (University of Toronto). The coiled-coiled domain (CCD) of human KIF22 was cloned in pHTC HaloTag CMV-neo

vector (gift from Dr Mark Dodding, King's College London, UK) between Nhe1 and XhoI sites, following primers were used for PCR: Sense-5'-AAAGCTAGCATGGACCGTCTGCTTGCCTC-3'; Antisense- 5'-CTCGAGTTGATCCAGTATTTTTTGGCGCC-3'.

Cell Culture

A549 human lung adenocarcinoma cells were grown in DMEM supplemented with 10% FCS. Cells expressing shRNA to target CAR were maintained in DMEM containing 10% FCS and 1.2μg/ml Puromycin. H1975 ^{WT} adenocarcinoma cells were grown in RPMI media with 10% FCS, 1.5 μg/ml Puromycin and 1mg/ml G418. HEK293 packaging cells were used to generate lentiviral particles for viral transduction as previously described (7). 16HBE human bronchial epithelial cells were a gift from Prof D.Gruenert (University of Vermont, US; (54)) and were cultured in MEM containing 10%FCS and supplemented with glutamine. All CAR expressing stable cell lines were produced using lentiviral expression as previously described (7, 26).

Confocal microscopy

Cultured cells were washed twice with PBS, fixed with 4% PFA in PBS for 10 min or ice-cold methanol for 2 min and permeabilised with 0.1% TritonX-100 for 10 min. Cells were incubated with primary antibodies for 2 hours and appropriate secondary antibodies conjugated to Alexafluor-568 or 488 and Phalloidin conjugated to Alexafluor 647, including Hoescht, for 1 hour. Cells stained using HaloTag TMR Direct Ligand were incubated live with the ligand overnight before fixation. Cells were mounted onto slides using Fluorsave (ICN). Confocal microscopy was performed using a Nikon A1R inverted confocal laser scanning microscope with a 60x oil objective and laser excitation wavelengths of 405nm, 488 nm, 561 nm and 633 nm.

Analysis of microtubule area

Images were all taken at the same laser settings and objectives using Nikon Imaging Software Elements and the same Nikon A1R confocal microscope. Actin, β-tubulin and nuclei channels were saved separately as TIFF files. These images were analysed using ICY software; images were thresholded to remove background, and the nucleus signal was merged with both the actin and β-tubulin signal. Masks were produced of these merged images and overlaid, following which the difference between the 2 masks was calculated to determine the number of pixels representing the actin signal without a corresponding β-tubulin signal. This value was converted to μm^2 to determine the surface area per field of view with actin present absent of β-tubulin.

Live imaging

For live cell imaging experiments, A549 were plated onto 6-well plastic plates (cell division assay) or glass-bottomed dishes (CAR junctional analysis, microtubule tracking) (Ibidi). For cell division assays, HEPES (25mM) was added to the cells which were then imaged every 5 min for 12 hours using phase contrast and 488 and 568 nm laser excitation using a 20X objective on an Olympus IX71 inverted fluorescence microscope equipped with a humidified

environmental chamber heated to 37 °C. All images were saved as avi files. For CAR junctional analysis cells were imaged every minute using 488 nm laser excitation using a 60x oil objective on a Nikon A1R inverted confocal microscope (Nikon UK) equipped with a humidified environmental chamber heated to 37 °C, with PFS activated. After 5 min, EGF was added to the imaging media at a final concentration of 10ng/ml and the imaging immediately resumed for a further 60 min. All images were saved as nd2 files and analysed in ImageJ or exported as tif files for presentation. For microtubule tracking assays, time-lapse movies of A549 cells expressing tubulin–GFP were acquired on an inverted Nikon A1R confocal laser scanning microscope using a 100× NA 1.45 oil objective at a rate of one frame per 2 seconds with or without EGF addition (10ng/ml). Images were saved as nd2 files and analyzed in ImageJ or exported as tif files for presentation.

Quantification of live imaging

To analyze cell division, the beginning of division was determined by morphological rounding of cells using phase contrast imaging, prior to DNA condensation determined by the H2BK-GFP or mCherry signal. The number of frames until the end of DNA separation or complete cell division (cell spreading of daughter cells) was quantified and used to determine the overall time of cell division. Cells were considered separated if less than a third of the cell boundaries of the daughter cells were attached to each other, this was analyzed up to 90 minutes post nuclear division. To analyze CAR localization at junctions, videos were opened in ImageJ and line scans (4.2μm) drawn perpendicular to junctions. The intensity profile of CAR-GFP was then calculated, 30 junctions were analysed per condition, which were then averaged and normalized. To analyze CAR-GFP and EGFR-mCherry dynamics in live cells, identically sized region-of-interest boxes were placed over central (5 μm-wide) junctional regions at time 0, and the resulting intensity measurements over time calculated for both GFP and mCherry channels. These values were then exported into Graphpad prism and normalized to the starting intensity for each junction analyzed to provide relative intensity changes over time. For analysis of single microtubules at the cell periphery (microtubule tracking assay), acquired movies were subjected to a bandpass filter (20:2 pixels) in ImageJ, background subtracted using a rolling ball radius of 15 pixels, and a 3D Gaussian blur filter was applied. Resulting movies were overlaid with the originals to avoid image- processing-derived artefacts and single microtubule growth was measured over time from a defined starting point proximal to the cell periphery. Frequency of catastrophe, growth rate and time spent in growth phase were quantified as in (55). Example representative images of time-dependent changes to microtubule dynamics were generated using the Temporal Colour Code plugin in FIJI (Centre for Molecular and Cellular Imaging, EMBL, Germany).

Western blotting and immunoprecipitation

Cells were lysed in sample buffer containing β-mercaptoethanol at room temperature. Lysates were subjected to SDS-PAGE and blotted using nitrocellulose membrane. Blots were blocked and probed using 3% milk/PBS-0.2%tween or 5%BSA/TBS-0.1%tween and quantified using ECL Plus Western blot detection system (GE Healthcare). For IP experiments, GFP, CAR-GFP A549 or WT A549 expressing FLAG-tagged constructs were lysed in IP lysis buffer (pH7.4 50 mM Tris, 150 mM NaCl, 1 mM EDTA, 1% Triton, 1%

NP40, PI cocktail). Lysates were incubated with 5μg anti-GFP or anti-FLAG antibody pre-bound to A/G agarose beads overnight before washing the beads with 1 ml IP lysis buffer 3 times. Immunocomplexes were separated using SDS-PAGE and immunoblotted for specified proteins. Where relevant for quantification purposes, phospho-proteins levels were normalized to levels of the same total protein prior to comparing between conditions.

Biotinylation assay

Cells were incubated for 40 min at 4°C with EZ-Link® Sulfo-NHS-SS-Biotin solution (Thermo Scientific) (0.5mg/ml in PBS). Surface biotinylation was then quenched with PBS containing 50 mM glycine. To initiate EGFR internalization, cells were incubated in OPTIMEM containing EGF for specified time periods at 37°C and then cell surface biotin was stripped using MesNa Buffer (50 mM 2- mercaptoethanesulfonic acid sodium salt (Sigma Aldrich) for 1 hour at 4°C. One sample of cells was left unstripped as a control for surface labelling efficiency. Cells were then lysed with RIPA Buffer containing protease inhibitor cocktail and phosphatase inhibitors (100 μM Vanandate and 1 μM calyculin A). Biotinylated proteins were then isolated by pull-down using NeutrAvidin Agarose resin (Thermo Scientific) overnight at 4°C. Samples were then boiled with equal volumes of SDS PAGE Sample Buffer and analyzed by immunoblotting. The level of internalised EGFR at different time points was determined as the % difference between non-MesNa-stripped cells and stripped cells and corrected for any variations of the total cell lysate protein of each sample.

Proliferation Assays

$5x10^3$ A549 or A549s expressing H2BK-GFP cells were plated into 12-well tissue culture plates and incubated for 24 or 48 hours. $8x10^3$ H1975 WT EGFR cells were plated into a sterile 12-well tissue culture plate, and incubated for 24, 48 or 72 hours. $8x10^4$ WT 16HBE or 16HBE stable cell lines expressing CAR-GFP or transfected with CAR-targeted siRNA or were plated into a sterile 12-well tissue culture plate and incubated for 24 or 48 hours. Hoechst was added to the media of the cells for 30 mins to stain DNA, and then cells were fixed for 15 mins in 4% PFA/PBS in the dark. Using a 10X objective on an Olympus IX71 inverted fluorescence microscope, cells were imaged using the same exposure with the 406nm laser, 6 images per well were saved as TIFF files. H2BK-GFP A549s were grown for 24 hours and using an Olympus IX71 inverted fluorescence microscope microscope (10X objective), cells were imaged live using the same exposure with the 488nm laser, 6 images per well were saved as TIFF files and then the cells were incubated for a further 24 hours following which they were imaged again. TIFF files were opened in ImageJ and the number of nuclei per image was analysed by thresholding nuclei followed by selecting based on size and circularity to determine the number of particles. The number of particles was counted per field enabling total number of nuclei to be calculated across multiple fields.

Agar colony assay

Agar plates were prepared by mixing complete growth media with 2% Noble Agar to produce a solution of 0.7% Agar. 1.5ml of the agar solution was added to a well of a sterile 6-well tissue culture plate, and incubated at room temperature for 30 min to set. $4x10^4$ A549 cells/well and $1x10^5$ wild-type H1975 cells were mixed with preheated 2% Noble Agar to

make a 0.3% agar solution and 1.5 ml was added to each well on top of the bottom agar layer. 1 ml of fresh growth media was then added over the top of the agar solution, and replaced every 2-3 days. A549 cells were grown for 2 weeks, wild-type H1975 cells were grown for 3 weeks, after which, colonies were fixed and stained for 30 minutes in a 0.5% Crystal Violet/ 20% methanol/ PBS. Colonies were imaged on an Olympus IX71 inverted fluorescence microscope (4X objective) and analyzed using ImageJ. Colony number and size was calculated in ImageJ.

Recombinant protein production and pulldowns

The cDNAs encoding the GST-NT and GST-CT KIF22 domains, were kindly provided by Andy Wilde (University of Toronto). BL21 cells containing DNA of interest were grown in 400ml of LB broth and cells grown at 37°C and then protein production was induced with Isopropyl β-D-1- thiogalactopyranoside (IPTG, 100μM) and incubated for a further 4 hours at 30°C. The bacterial culture was pelleted and frozen overnight at -80°C and then lysed in 50μl ice cold PBS per ml of original culture volume, containing protease inhibitors (Calbiochem). Bacterial pellets were disrupted by sonication for 2 minutes, using 10-second pulses at 10A on ice. The solution was centrifuged and the supernatant collected and filtered using a 0.45μm filter. Pre-washed glutathione Sepharose 4B beads (GE Healthcare) were added to the supernatant to 1μl beads/1ml original culture and left to mix overnight at 4°C. The beads were washed twice with PBS contained 0.4M NaCl and 1% Brijj and resuspended in 1ml buffer with protease inhibitors. SDS-PAGE and coomassie blue analysis was run to confirm protein purification. A549 or HEK-293T cells were washed and scraped into cold lysis buffer (50 mM Tris (pH7.2), 150 mM NaCl, 20mM EDTA, 1% NP40, 1% Triton X-100), containing protease inhibitor cocktail and phosphatase inhibitors (100 μM Vanandate and 1 μM calyculin A). Lysates were then centrifuged to pellet insoluble material. A sample of cell lysate was removed before adding lysate to beads to allow analysis of total protein. The cleared lysates were transferred into tubes with 50μl GST-tagged protein and placed on a rotator at 4°C overnight. The beads were washed 4 times with ice-cold lysis buffer. After the final wash, the wash buffer was removed and SDS sample buffer was added. The sample was boiled and run on a 12% acrylamide gel and analyzed by immunoblotting.

In vivo tumorigenicity assays

H1975WT control (siCtrl) or CAR KD (siCAR1 and siCAR2) cell lines ($3x10^6$) were injected subcutaneously into the two posterior flanks of BALB/c nude mice (Charles River Laboratories). 9 female 5 week-old mice in total were used for control cell lines and 5 for each siRNA. Mice were followed daily and tumors were measured with a caliper in long and short axes and volume was determined in based of the equation 0.4xAxB^2 (A, the long axis and B, the short axis of the tumor). At day 14th after injection mice were culled using CO_2 and tumours were removed aseptically with dissecting scissors and weighed. All animals were maintained under specific pathogen-free conditions and handled in accordance with the Institutional Committees on Animal Welfare of the UK Home Office (The Home Office Animals Scientific Procedures Act, 1986). All animal experiments were approved by the Ethical Review Process Committee at King's College London and carried out under license from the Home Office, UK.

Tissue samples, immunohistochemistry and histopathological analysis

Tissue samples obtained from xenografts were fixed with formalin and paraffin-embedded. Immunohistochemical analyses were performed using 3 mm sections. Briefly, slides were dewaxed and antigen retrieval was performed using 0.1M citrate pH 6.0 buffer at 120°C for 10 min, followed by blocking in TBS-Tween 0.1% + 1% BSA + 1% FBS. Primary antibodies were added overnight at 4 ºC. Peroxidase-conjugated (Envision+) anti-rabbit and anti-mouse Ig reagents from Dako were used as secondary antibodies for 1h. Non-immune (Santa Cruz Biotechnology) or pre-immune rabbit serum was used as negative controls. Reactions were developed using diaminobenzidine (DAB) as chromogenic substrate. Images from digitalized scans of the glass slide specimens were obtained at magnification ×20 (0.45 μm/pixel resolution) using a Hamamatsu Nanozoomer 2.0 HT. All quantification was performed in Image J.

Statistical analysis

All statistical tests were performed using Students t-tests or two-way ANOVA (GraphPad Prism). Correlation analysis was performed using Pearsons' Correlation Coefficient (ImageJ).

Supplementary Material

Refer to Web version on PubMed Central for supplementary material.

Acknowledgments

The authors would like to thank Dr Maddika Subba Reddy (CDFD, Hyderabad, India) and Dr Andy Wilde (University of Toronto) for the kind gifts of KIF22 plasmids.

Funding: The authors acknowledge funding from King's Health Partners, National Institute for Health Research (NIHR) Clinical Research Facility and NIHR Biomedical Research Centre based at Guy's and St Thomas' NHS Foundation Trust, King's College London and the BBSRC (BB/M503320/1).

References

1. Bergelson JM, et al. Isolation of a common receptor for Coxsackie B viruses and adenoviruses 2 and 5. Science. 1997; 275:1320–1323. [PubMed: 9036860]
2. Cohen CJ, et al. The coxsackievirus and adenovirus receptor is a transmembrane component of the tight junction. Proc Natl Acad Sci U S A. 2001; 98:15191–15196. [PubMed: 11734628]
3. Raschperger E, et al. The coxsackie- and adenovirus receptor (CAR) is an in vivo marker for epithelial tight junctions, with a potential role in regulating permeability and tissue homeostasis. Exp Cell Res. 2006; 312:1566–1580. [PubMed: 16542650]
4. Schmitz H, et al. Altered tight junction structure contributes to the impaired epithelial barrier function in ulcerative colitis. Gastroenterology. 1999; 116:301–309. [PubMed: 9922310]
5. Coyne CB, Bergelson JM. CAR: a virus receptor within the tight junction. Adv Drug Deliv Rev. 2005; 57:869–882. [PubMed: 15820557]
6. Hussain F, et al. CAR modulates E-cadherin dynamics in the presence of adenovirus type 5. PLoS One. 2011; 6:e23056. [PubMed: 21850251]
7. Morton PE, Hicks A, Nastos T, Santis G, Parsons M. CAR regulates epithelial cell junction stability through control of E-cadherin trafficking. Sci Rep. 2013; 3:2889. [PubMed: 24096322]

8. Chen Z, et al. Expression of the coxsackie and adenovirus receptor in human lung cancers. Tumour biology : the journal of the International Society for Oncodevelopmental Biology and Medicine. 2013; 34:17–24. [PubMed: 23307165]
9. Veena MS, Qin M, Andersson A, Sharma S, Batra RK. CAR mediates efficient tumor engraftment of mesenchymal type lung cancer cells. Laboratory investigation; a journal of technical methods and pathology. 2009; 89:875–886. [PubMed: 19506548]
10. Saito K, et al. Coxsackie and adenovirus receptor is a critical regulator for the survival and growth of oral squamous carcinoma cells. Oncogene. 2014; 33:1274–1286. [PubMed: 23503462]
11. Lacher MD, et al. ZEB1 limits adenoviral infectability by transcriptionally repressing the coxsackie virus and adenovirus receptor. Mol Cancer. 2011; 10:91. [PubMed: 21791114]
12. Yamashita M, Ino A, Kawabata K, Sakurai F, Mizuguchi H. Expression of coxsackie and adenovirus receptor reduces the lung metastatic potential of murine tumor cells. Int J Cancer. 2007; 121:1690–1696. [PubMed: 17546646]
13. Qin M, Escuadro B, Dohadwala M, Sharma S, Batra RK. A novel role for the coxsackie adenovirus receptor in mediating tumor formation by lung cancer cells. Cancer Res. 2004; 64:6377–6380. [PubMed: 15374942]
14. Zhang X, Fang B, Mohan R, Chang JY. Coxsackie-adenovirus receptor as a novel marker of stem cells in treatment-resistant non-small cell lung cancer. Radiother Oncol. 2012; 105:250–257. [PubMed: 23022172]
15. Hodkinson PS, Mackinnon A, Sethi T. Targeting growth factors in lung cancer. Chest. 2008; 133:1209–1216. [PubMed: 18460519]
16. Ladanyi M, Pao W. Lung adenocarcinoma: guiding EGFR-targeted therapy and beyond. Mod Pathol. 2008; 21(Suppl 2):S16–22. [PubMed: 18437168]
17. Lemmon MA, Schlessinger J. Cell signaling by receptor-tyrosine kinases. Cell. 2010; 141:1117–1134. [PubMed: 20602996]
18. Pece S, Gutkind JS. Signaling from E-cadherins to the MAPK pathway by the recruitment and activation of epidermal growth factor receptors upon cell-cell contact formation. J Biol Chem. 2000; 275:41227–41233. [PubMed: 10969083]
19. Petecchia L, et al. Cytokines induce tight junction disassembly in airway cells via an EGFR-dependent MAPK/ERK1/2-pathway. Lab Invest. 2012; 92:1140–1148. [PubMed: 22584669]
20. Wang Y, et al. Tyrosine phosphorylated Par3 regulates epithelial tight junction assembly promoted by EGFR signaling. EMBO J. 2006; 25:5058–5070. [PubMed: 17053785]
21. Singh AB, Harris RC. Epidermal growth factor receptor activation differentially regulates claudin expression and enhances transepithelial resistance in Madin-Darby canine kidney cells. J Biol Chem. 2004; 279:3543–3552. [PubMed: 14593119]
22. Bae GY, et al. Loss of E-cadherin activates EGFR-MEK/ERK signaling, which promotes invasion via the ZEB1/MMP2 axis in non-small cell lung cancer. Oncotarget. 2013; 4:2512–2522. [PubMed: 24318272]
23. Salinas S, et al. Disruption of the coxsackievirus and adenovirus receptor-homodimeric interaction triggers lipid microdomain- and dynamin-dependent endocytosis and lysosomal targeting. J Biol Chem. 2014; 289:680–695. [PubMed: 24273169]
24. Deribe YL, et al. Regulation of epidermal growth factor receptor trafficking by lysine deacetylase HDAC6. Sci Signal. 2009; 2:ra84. [PubMed: 20029029]
25. Erasmus JC, Welsh NJ, Braga VM. Cooperation of distinct Rac-dependent pathways to stabilise E-cadherin adhesion. Cell Signal. 2015; 27:1905–1913. [PubMed: 25957131]
26. Morton PE, et al. TNFalpha promotes CAR-dependent migration of leukocytes across epithelial monolayers. Sci Rep. 2016; 6:26321. [PubMed: 27193388]
27. Maddika S, Sy SM, Chen J. Functional interaction between Chfr and Kif22 controls genomic stability. J Biol Chem. 2009; 284:12998–13003. [PubMed: 19321445]
28. Truebestein L, Leonard TA. Coiled-coils: The long and short of it. Bioessays. 2016; 38:903–916. [PubMed: 27492088]
29. Levesque AA, Compton DA. The chromokinesin Kid is necessary for chromosome arm orientation and oscillation, but not congression, on mitotic spindles. J Cell Biol. 2001; 154:1135–1146. [PubMed: 11564754]

30. Tokai-Nishizumi N, Ohsugi M, Suzuki E, Yamamoto T. The chromokinesin Kid is required for maintenance of proper metaphase spindle size. Mol Biol Cell. 2005; 16:5455–5463. [PubMed: 16176979]
31. Yu Y, et al. Inhibition of KIF22 suppresses cancer cell proliferation by delaying mitotic exit through upregulating CDC25C expression. Carcinogenesis. 2014; 35:1416–1425. [PubMed: 24626146]
32. Tomas A, Futter CE, Eden ER. EGF receptor trafficking: consequences for signaling and cancer. Trends Cell Biol. 2014; 24:26–34. [PubMed: 24295852]
33. Sousa LP, et al. Suppression of EGFR endocytosis by dynamin depletion reveals that EGFR signaling occurs primarily at the plasma membrane. Proc Natl Acad Sci U S A. 2012; 109:4419–4424. [PubMed: 22371560]
34. Jones S, Rappoport JZ. Interdependent epidermal growth factor receptor signalling and trafficking. Int J Biochem Cell Biol. 2014; 51:23–28. [PubMed: 24681003]
35. Sigismund S, et al. Clathrin-mediated internalization is essential for sustained EGFR signaling but dispensable for degradation. Dev Cell. 2008; 15:209–219. [PubMed: 18694561]
36. Liu W, et al. HDAC6 regulates epidermal growth factor receptor (EGFR) endocytic trafficking and degradation in renal epithelial cells. PLoS One. 2012; 7:e49418. [PubMed: 23152903]
37. Park SM, Littleton JT, Park HR, Lee JH. Drosophila Homolog of Human KIF22 at the Autism-Linked 16p11.2 Loci Influences Synaptic Connectivity at Larval Neuromuscular Junctions. Exp Neurobiol. 2016; 25:33–39. [PubMed: 26924931]
38. Mukhopadhyay B, Nam SC, Choi KW. Kinesin II is required for cell survival and adherens junction positioning in Drosophila photoreceptors. Genesis. 2010; 48:522–530. [PubMed: 20506262]
39. Hein MY, et al. A human interactome in three quantitative dimensions organized by stoichiometries and abundances. Cell. 2015; 163:712–723. [PubMed: 26496610]
40. Ligon LA, Karki S, Tokito M, Holzbaur EL. Dynein binds to beta-catenin and may tether microtubules at adherens junctions. Nat Cell Biol. 2001; 3:913–917. [PubMed: 11584273]
41. Yano T, Matsui T, Tamura A, Uji M, Tsukita S. The association of microtubules with tight junctions is promoted by cingulin phosphorylation by AMPK. J Cell Biol. 2013; 203:605–614. [PubMed: 24385485]
42. Gomez GA, McLachlan RW, Yap AS. Productive tension: force-sensing and homeostasis of cell-cell junctions. Trends Cell Biol. 2011; 21:499–505. [PubMed: 21763139]
43. Jaqaman K, et al. Cytoskeletal control of CD36 diffusion promotes its receptor and signaling function. Cell. 2011; 146:593–606. [PubMed: 21854984]
44. Verhey KJ, Hammond JW. Traffic control: regulation of kinesin motors. Nat Rev Mol Cell Biol. 2009; 10:765–777. [PubMed: 19851335]
45. Soeda S, Yamada-Nomoto K, Ohsugi M. The microtubule-binding and coiled-coil domains of Kid are required to turn off the polar ejection force at anaphase. J Cell Sci. 2016; 129:3609–3619. [PubMed: 27550518]
46. Ohsugi M, et al. Cdc2-mediated phosphorylation of Kid controls its distribution to spindle and chromosomes. EMBO J. 2003; 22:2091–2103. [PubMed: 12727876]
47. Hoepfner S, et al. Modulation of receptor recycling and degradation by the endosomal kinesin KIF16B. Cell. 2005; 121:437–450. [PubMed: 15882625]
48. Wang Y, Pennock S, Chen X, Wang Z. Endosomal signaling of epidermal growth factor receptor stimulates signal transduction pathways leading to cell survival. Mol Cell Biol. 2002; 22:7279–7290. [PubMed: 12242303]
49. Mayr MI, Storch M, Howard J, Mayer TU. A non-motor microtubule binding site is essential for the high processivity and mitotic function of kinesin-8 Kif18A. PLoS One. 2011; 6:e27471. [PubMed: 22102900]
50. Stumpff J, et al. A tethering mechanism controls the processivity and kinetochore-microtubule plus-end enrichment of the kinesin-8 Kif18A. Mol Cell. 2011; 43:764–775. [PubMed: 21884977]
51. Boggara M, Athmakuri K, Srivastava S, Cole R, Kane RS. Characterization of the diffusion of epidermal growth factor receptor clusters by single particle tracking. Biochim Biophys Acta. 2013; 1828:419–426. [PubMed: 22974816]

52. Wu X, et al. Microtubule inhibition causes epidermal growth factor receptor inactivation in oesophageal cancer cells. Int J Oncol. 2013; 42:297–304. [PubMed: 23174948]
53. Vicente JJ, Wordeman L. Mitosis, microtubule dynamics and the evolution of kinesins. Exp Cell Res. 2015; 334:61–69. [PubMed: 25708751]
54. Cozens AL, et al. CFTR expression and chloride secretion in polarized immortal human bronchial epithelial cells. Am J Respir Cell Mol Biol. 1994; 10:38–47. [PubMed: 7507342]
55. Villari G, et al. A direct interaction between fascin and microtubules contributes to adhesion dynamics and cell migration. J Cell Sci. 2015; 128:4601–4614. [PubMed: 26542021]

Europe PMC Funders Author Manuscripts

Europe PMC Funders Author Manuscripts

One-sentence summary

The cell junction-associated receptor CAR coordinates the dynamics between EGFR signaling and the cytoskeleton during cell proliferation.

Europe PMC Funders Author Manuscripts

Editor's summary

The EGFR-cytoskeleton connection

Growth factor signaling stimulates cell proliferation and migration, which requires changes in cell-cell adhesion and the cytoskeleton. Increased activity of the growth factor receptor EGFR is implicated in various cancers. Pike *et al.* found that EGFR signaling directs changes in cell-cell junctions and the cytoskeleton in lung cancer cells by inducing the phosphorylation of the cell adhesion receptor CAR. Phosphorylated CAR interacted with the microtubule motor protein KIF22 to stabilize the peripheral microtubule network, which facilitated cell division and anchorage-independent growth associated with metastasis. It also altered the trafficking of EGFR such that its signaling was prolonged. Thus, CAR or KIF22 might be alternative targets for therapeutically inhibiting EGFR signaling in some cancers.

Europe PMC Funders Author Manuscripts

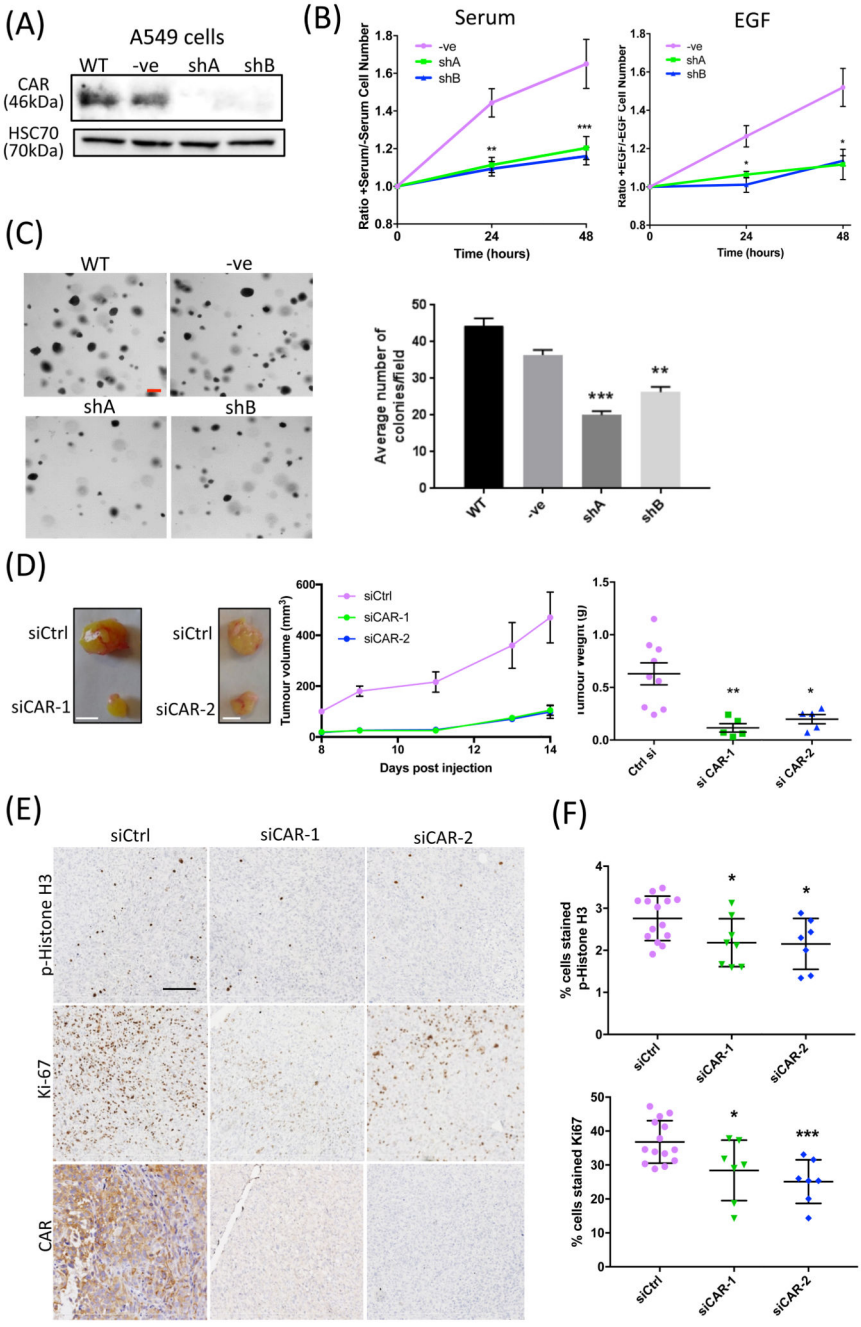

Figure 1. CAR regulates lung cancer cell proliferation in vitro and in vivo

(A) Western blot of CAR KD in A549 cells, either untransfected (WT) or transfected with control shRNA (-ve) or one of two shRNA sequences targeting *CAR* (shA and shB). **(B)** A549 cell proliferation over 48 hours in response to serum (left) or EGF (10 ng/ml; right). Data is normalized to serum-free control samples for both. Data are from 3 independent experiments. **(C)** Left: Representative images (left) and analysis (right) of agar colony growth assays in A549 control or CAR KD cells (shA, shB). Scale bars are 100μm. Data are average number of colonies per field in all cells from 10 fields per cell line, and are

representative of 3 independent experiments. **(D)** Representative images of resected tumours from xenograft models using H1975 control or CAR KD cells. Graphs on right show tumour volume and weight over time in 9 (control), 5 (siCAR1) or 5 (siCAR2) mouse models, pooled from two independent experiments. **(E)** Example images of phospho-HistoneH3 (top) and Ki-67 (bottom) staining in xenograft tissues from H1975 cell tumours in (D). Scale bars are 50μm. (F) Analysis of the p-Histone H3 and Ki-67 staining in xenografts represented in (E). N≥12 tumours per condition over 2 independent experiments. Data in all graphs are mean ± SEM. *p<0.01, **p0.005 by 2-way ANOVA.

Europe PMC Funders Author Manuscripts

Europe PMC Funders Author Manuscripts

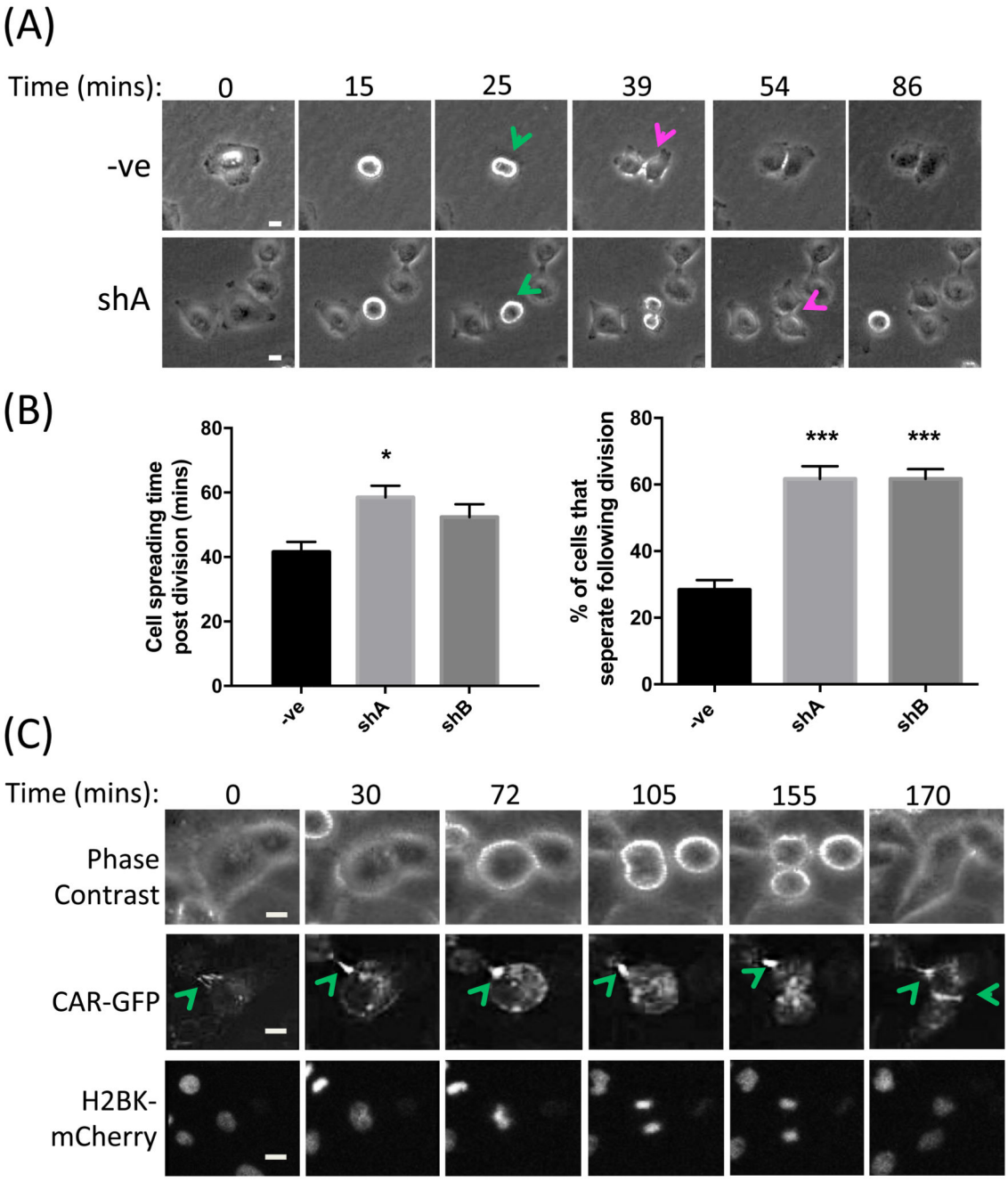

Figure 2. CAR promotes post-mitotic daughter cell attachment and spreading

(A) Representative images from time-lapse movies of shControl or CAR-KD (shA) A549 cells undergoing division. Green arrows denote dividing cells, red arrows denote initiation of daughter cell separation following division. **(B)** Quantification of time-lapse movies of control and CAR-KD cells (shA, shB) represented in (A), assessing the time taken for cells to re-spread post-division (left) and the percentage of cells that separate completely after division (right). Data are quantified from at least 20 cells over 3 independent experiments. Data are mean ± SEM. *p<0.05, ***p<0.005. **(C)** Representative images from time-lapse

movies of A549 cells expressing CAR-GFP and H2BK-mCherry; n = 4 experiments. Green arrows denote sites of high CAR-GFP at cell-cell contact points. Scale bars are 10um.

Europe PMC Funders Author Manuscripts

Europe PMC Funders Author Manuscripts

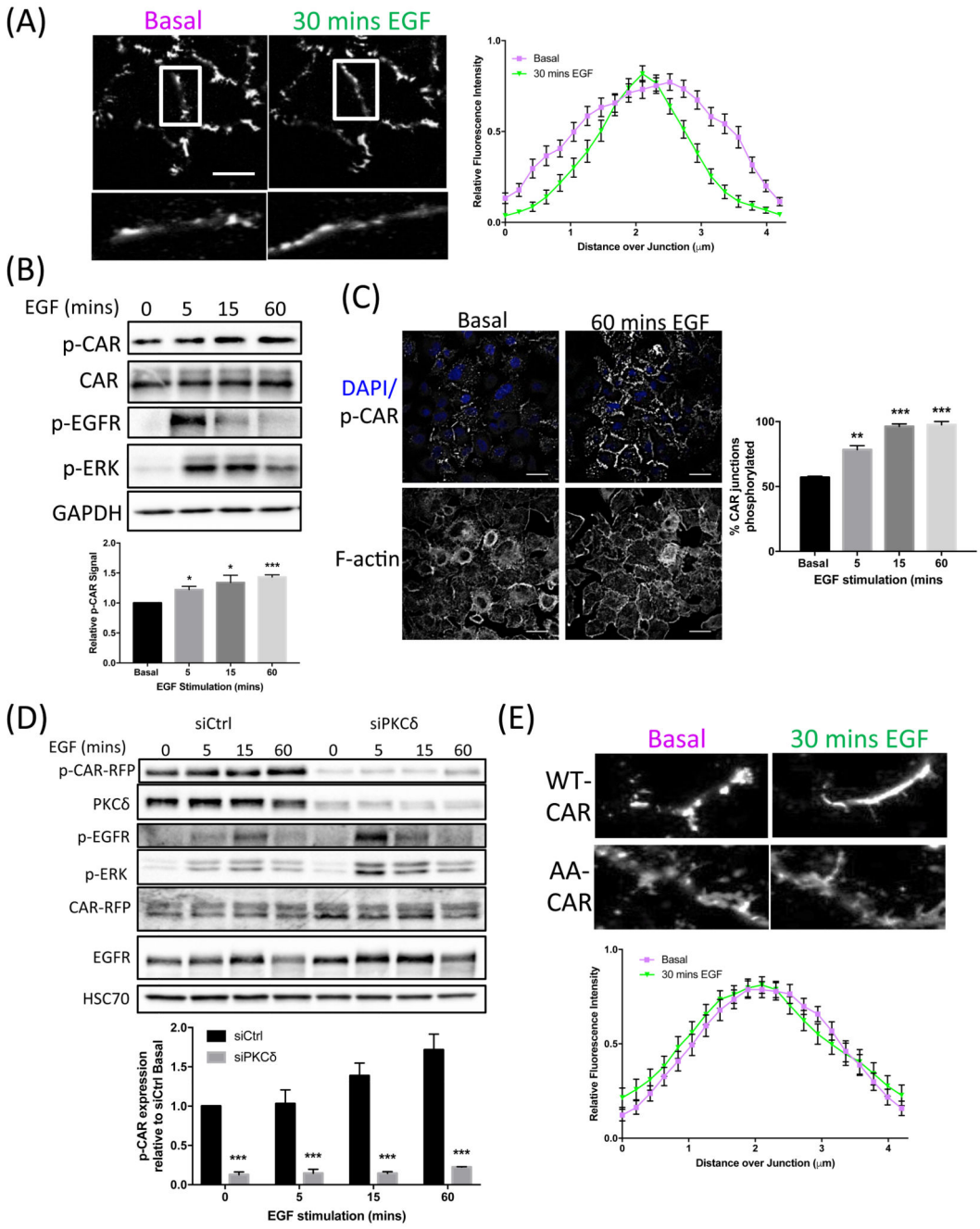

Figure 3. CAR is phosphorylated in response to EGF, leading to CAR movement within cell junctions

(A) Representative images from time-lapse movies of A549 cells expressing CAR-GFP at time 0 (untreated; top panels) versus 30 mins post-EGF addition (10 ng/ml; bottom panels). Graph shows quantification of CAR intensity at junctions measured at 0 and 30 min time points (example analysis areas shown in zoomed regions in images on left). Data is pooled from >20 junctions from at least 3 independent experiments, presented as mean ± SEM. **(B)** Western blots of lysates of A549 cells treated with EGF (10 ng/ml) for the specified times and probed for the specified proteins. Graph shows quantification of p-CAR abundance

(normalized to total CAR levels) relative to time 0 from 3 independent experiments. Data is presented as mean ± SEM. *p<0.05, **p<0.005. **(C)** Representative confocal images of A549 cells fixed after 0 or 60 mins of EGF stimulation (10 ng/ml) and stained for DAPI (blue, top images), phospho-CAR (white, top images) and actin (bottom images). Graph shows quantification of p-CAR staining from images at 5, 15 and 60 min after EGF stimulation from 100 cells per condition, presented as mean ± SEM. *p<0.05; ***p<0.005. **(D)** Western blots of control or PKCδKD A549 cells treated with EGF for specified time periods and probed for specified antibodies. Graph shows quantification of p-CAR levels relative to time 0 from 3 independent experiments, presented as mean ± SEM. **p<0.005. **(E)** Representative images from time-lapse movies of A549 cells expressing wild-type (WT) CAR-GFP (top panels) or AA-CAR-GFP (bottom panels) at 0 and 30 mins post-EGF stimulation. Graphs show analysis of AA-CAR-GFP movement at junctions as in (A), presented as mean ± SEM. All data were analyzed for statistical differences using 2-way ANOVA.

Europe PMC Funders Author Manuscripts

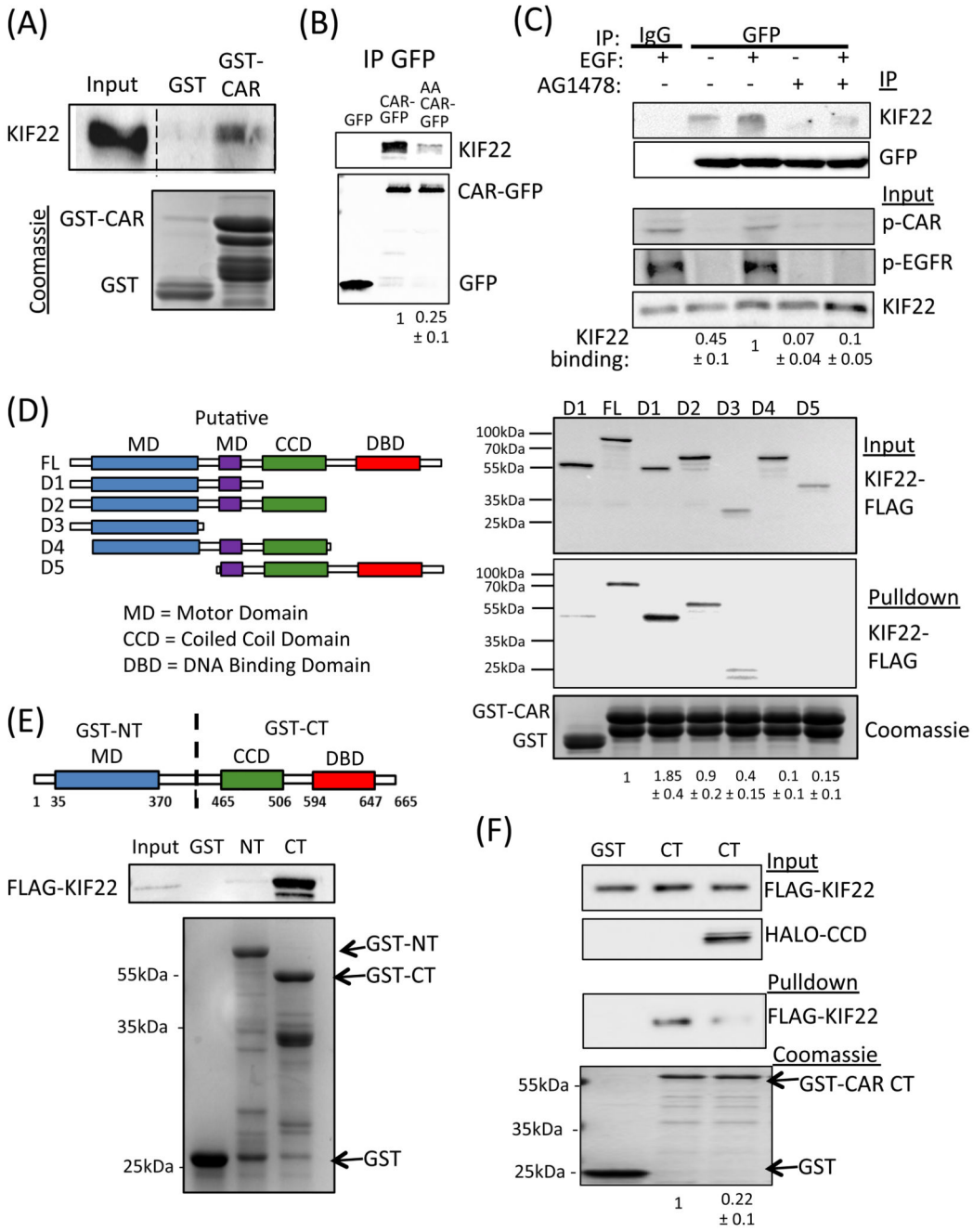

Figure 4. CAR binds to KIF22

(A) Representative blot of pulldowns using GST-tagged cytoplasmic domain of CAR incubated with lysates from A549 cells and probed for KIF22. GST alone was used a control. Bottom gel is Coomassie-stained equivalent gel showing input. **(B)** Representative blots of A549 cells expressing GFP, WT CAR-GFP or AA CAR-GFP and subjected to GFP immunoprecipitation. Blots were probed for KIF22 or GFP as indicated. **(C)** A549 cells expressing CAR-GFP were serum-starved (-) or EGF-stimulated (15min, 10 ng/ml; +) in the presence or absence of AG1478 and subjected to GFP IP followed by probing for specified

proteins. Top two panels show IP complexes, bottom three panels show input lysates. Quantification of KIF22 levels in IP complexes below blots are mean values from 3 independent experiments ± SEM. **(D)** Schematic cartoon of FLAG-tagged KIF22 constructs used for binding analysis. Right panel shows representative levels of KIF22-FLAG binding to GST-CAR cytoplasmic domain after pulldown from transfected HEK293 cell lysates. Coomassie-stained gel at bottom shows protein input. Quantification of KIF22 binding is provided beneath and represent mean values from 4 independent experiments ± SEM. **(E)** Schematic cartoon of GST-tagged N-terminal and C-terminal KIF22 constructs used for pulldowns. Blots beneath show representative results from pulldowns of KIF22-FLAG-expressing HEK293T cell lysates using N- or C-GST-KIF22. Data are representative of 5 independent experiments. **(F)** Representative blots from GST-tagged KIF22 C-terminal pulldowns from cell lysates expressing KIF22-FLAG in the presence or absence of co-expressed KIF22-CCD-HALO. GST was used as a control. Coomassie-stained gel at bottom shows protein input. Values beneath show levels of KIF22-FLAG in pulldowns and represent mean values from 3 independent experiments ± SEM. All data was analyzed for statistical differences using 2-way ANOVA.

Europe PMC Funders Author Manuscripts

Europe PMC Funders Author Manuscripts

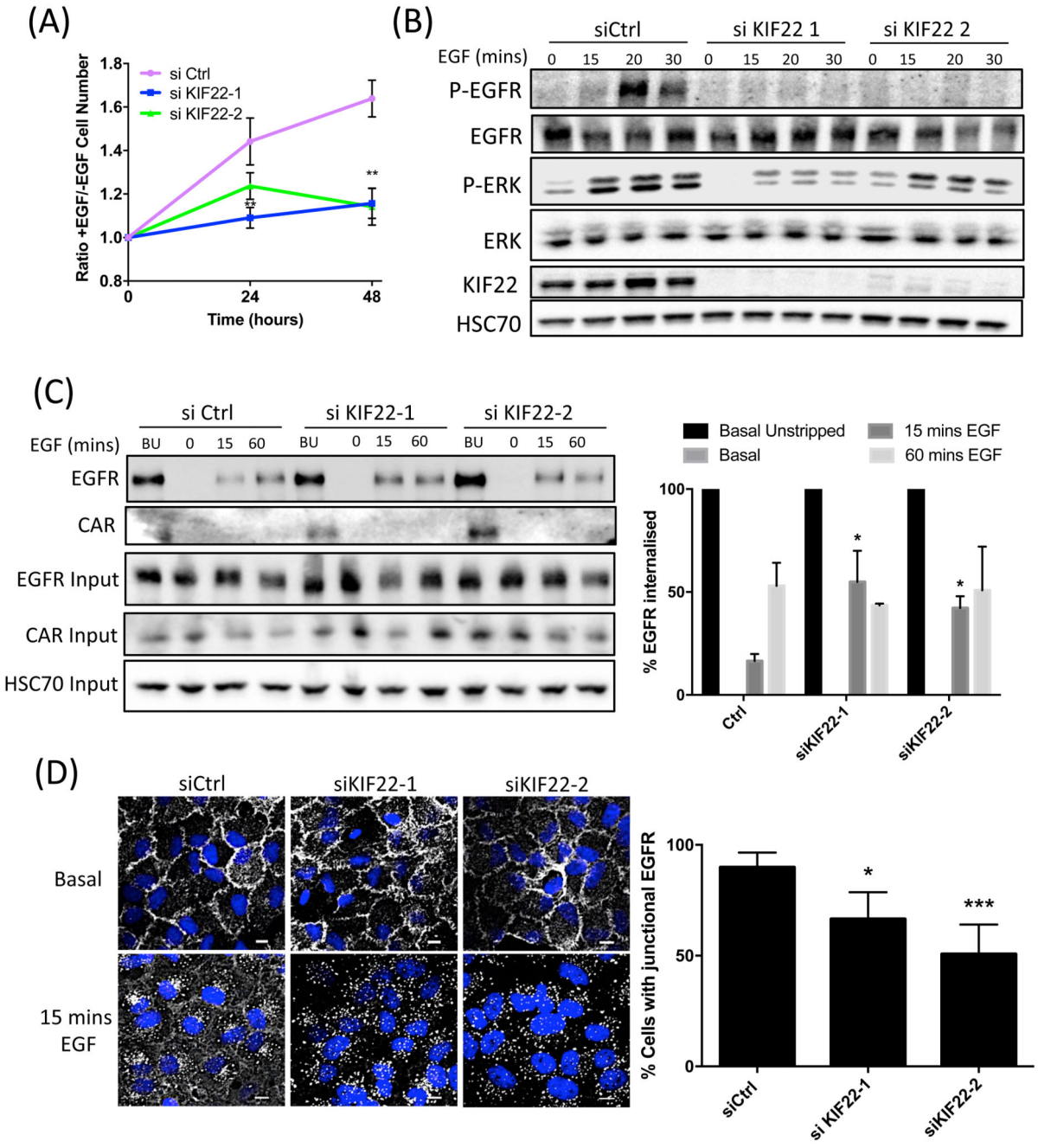

Figure 5. KIF22 promotes EGFR retention at plasma membrane and signalling in response to EGF

(A) Analysis of the proliferation of A549 cells transfected with control or one of two *KIF22*-targeted siRNAs and treated with EGF, quantified relative to serum-starved control cells. Data are mean ± SEM. **p<0.005. **(B)** Representative blots of lysates from control or KIF22-KD A549 cells treated with EGF over the specified time periods and probed with the specified antibodies. **(C)** Representative blots of surface biotinylation experiments showing the amount of surface EGFR (basal unstripped; BU) and internalized EGFR after 0, 15 and

60 mins EGF (10 ng/ml) in control or KIF22-KD A549 cells. Blots were probed with specified antibodies. Data in graph, right, were normalized to basal unstrapped (black bars) and are presented as mean ± SEM from 4 independent experiments. *=p<0.01 vs equivalent time point in Ctrl samples. **(D)** Representative images of control or KIF22-KD A549 cells, either untreated or after stimulation with EGF (10 ng/ml for 15 mins), fixed and stained for DAPI (blue) and EGFR (white). Scale bars are 10um. Graph on right shows quantification of junctional EGFR levels after stimulation with EGF. Data are mean ± SEM from 30 cells across 3 independent experiments. *p<0.01, ***p<0.001. All data analyzed for statistical differences using 2-way ANOVA.

Europe PMC Funders Author Manuscripts

Europe PMC Funders Author Manuscripts

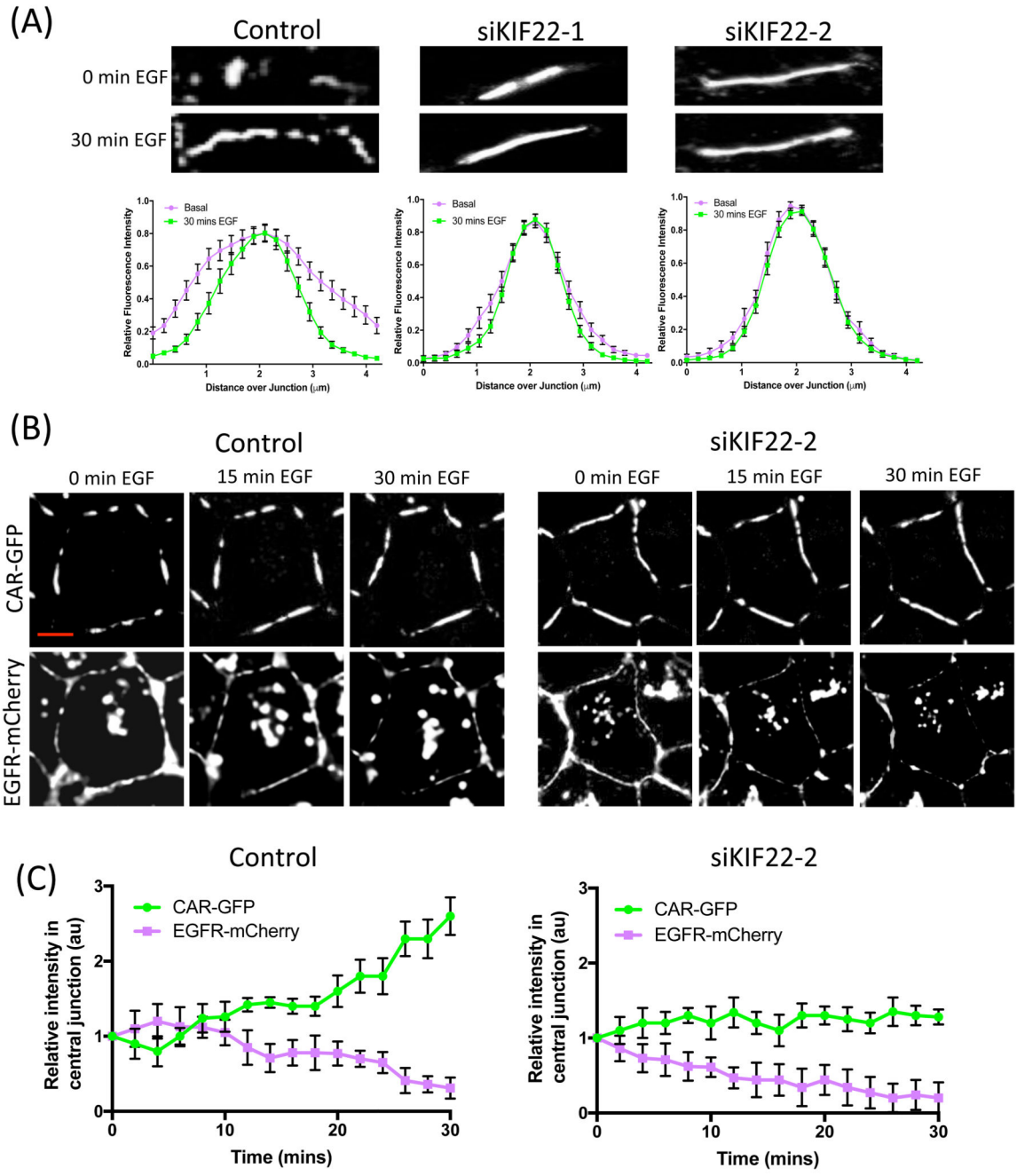

Figure 6. KIF22 regulates EGF-dependent movement of EGFR and CAR within junctions

(A) Representative images of CAR-GFP from time-lapse movies of control or KIF22-KD A549 cells expressing CAR-GFP, either untreated or after 30 mins EGF stimulation. CAR-GFP movement into junctions was quantified as described in Fig. 3 (A and E) and is presented as mean ± SEM. **(B)** Representative images of stills taken at specified time points after EGF treatment from time-lapse confocal movies of A549 cells co-expressing CAR-GFP (top), EGFR-mCherry (bottom) and control or KIF22 siRNA. **(C)** Quantification of movies as in (B) showing intensity of CAR-GFP (green) and EGFR-mCherry (red) at

junctions over time after stimulation with EGF. Data are mean ± SEM from 60 cells across 3 independent experiments. All data was analyzed for statistical differences using 2-way ANOVA.

Europe PMC Funders Author Manuscripts

Europe PMC Funders Author Manuscripts

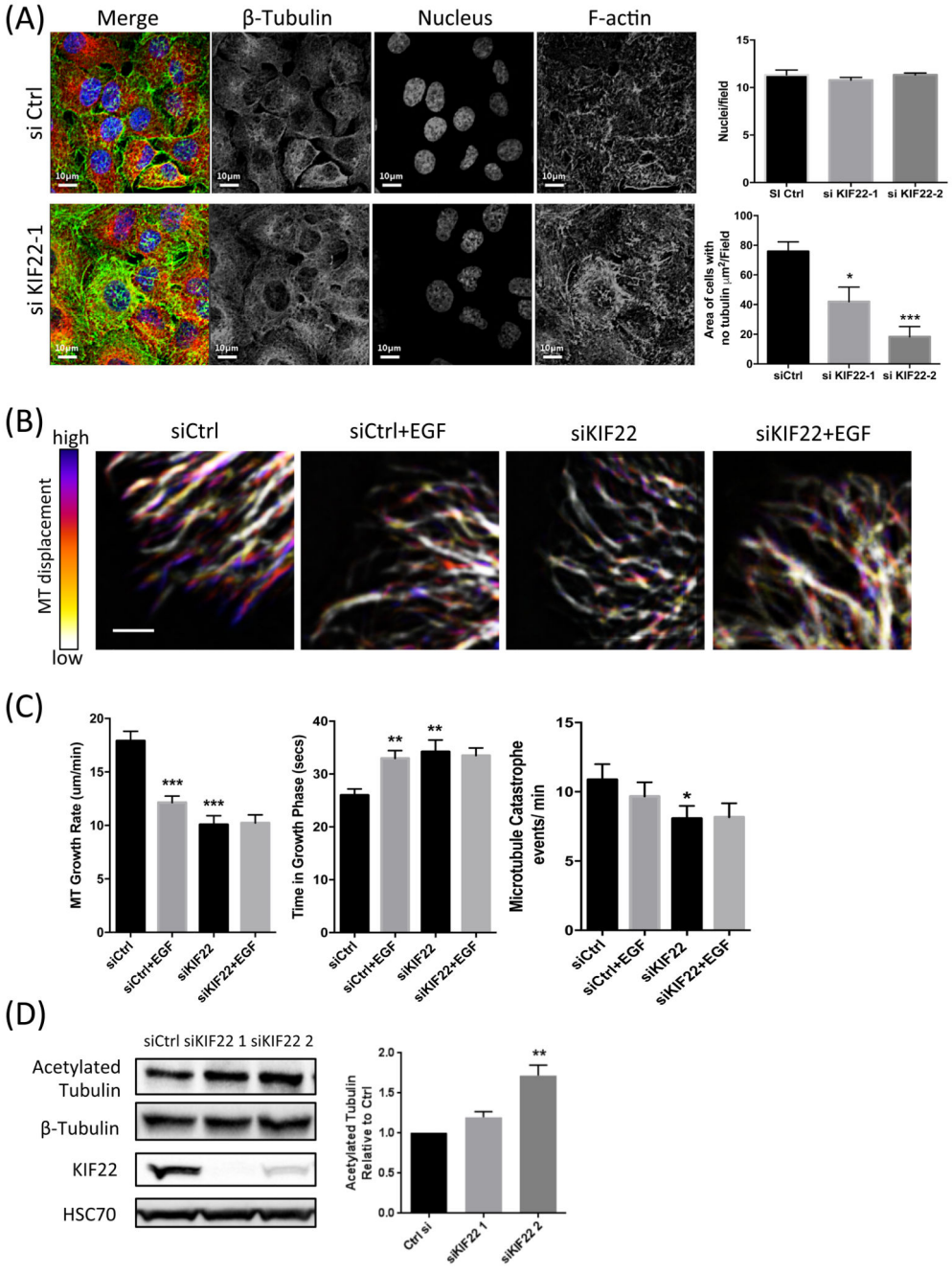

Figure 7. KIF22 regulates microtubule organisation and dynamics in cells in interphase

(A) Representative examples of confocal images of control or KIF22-KD A549 cells, fixed and stained for DAPI (nucleus; blue), β-tubulin (red) or F-actin (phalloidin; green). Scale bars are 10μm. Graphs show number of nuclei per field and area of cells with no tubulin staining present represented as area (μm^2/field). Data are mean ± SEM pooled from 9 fields per condition across 3 independent experiments. *p<0.01; ***p<0.001. **(B)** Representative example images from time-lapse movies of GFP-tubulin expressed in control or KIF22-KD A549 cells after stimulation with EGF. Time-dependent changes are depicted as color scales

from time-projected stacks in which blue represents regions of highly dynamic microtubule (MT) growth and white denotes regions of static or disassembling microtubules. Scale bar is 2 μm. **(C)** Analysis of microtubule growth rate (μm/min), time spent in growth phase (secs), and catastrophe events per min in control or KIF22-KD cells, with and without EGF (10ng/ml). Data are mean ± SEM pooled from 22 cells total across 2 independent experiments. **p<0.005, ***p<0.001. **(D)** Representative western blot of acetylated tubulin in control and KIF22-KD cells. Data on right are mean ± SEM from 4 independent experiments. **p<0.005. All data was analyzed for statistical differences using 2-way ANOVA.

Europe PMC Funders Author Manuscripts

Europe PMC Funders Author Manuscripts

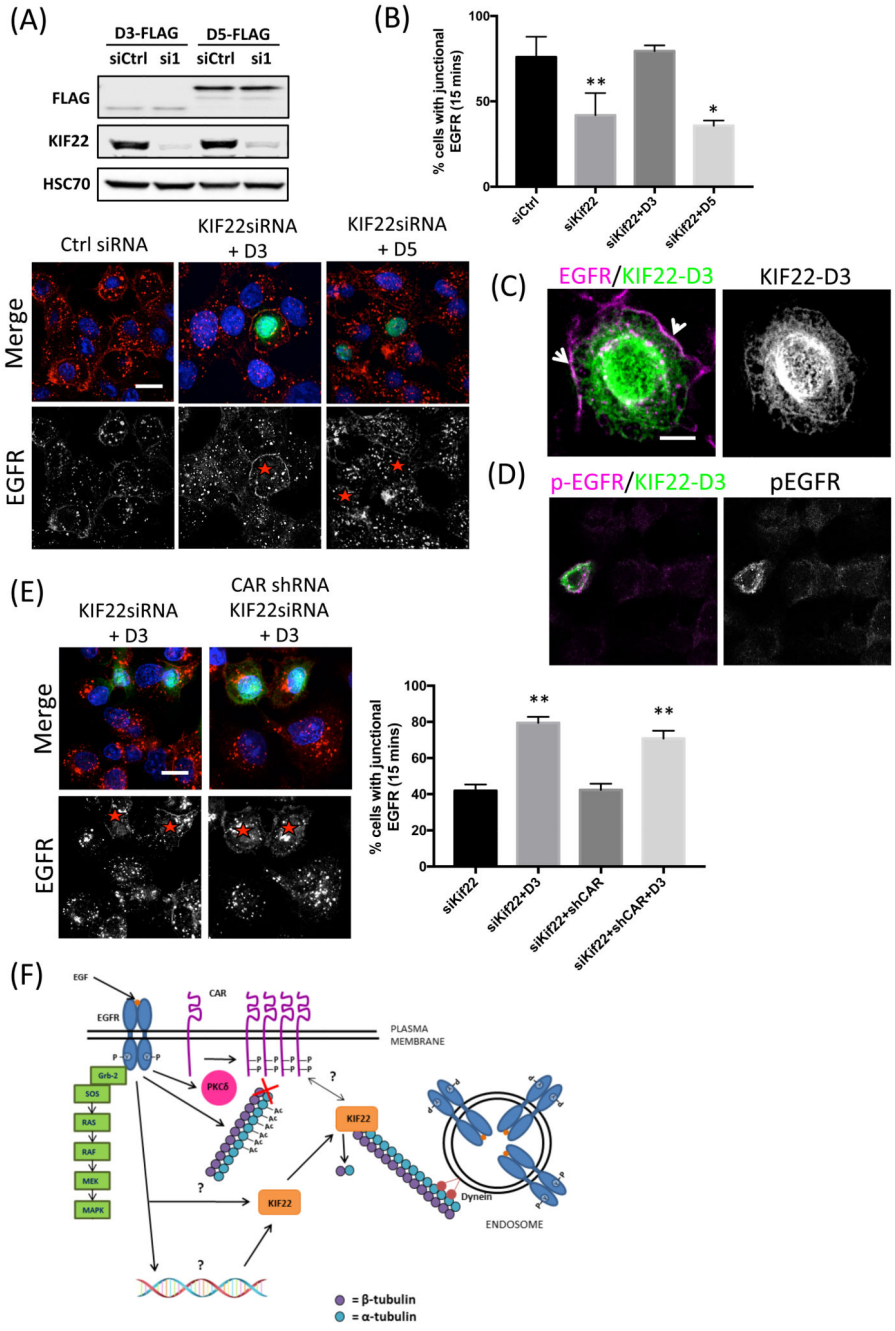

Figure 8. Cytoplasmic KIF22 sustains EGFR at the plasma membrane

(A) Top, Western blot assessing the efficiency of KIF22-KD and re-expression. Bottom, representative images of control (siCtrl) or KIF22 siRNA-treated A549 cells co-expressing FLAG-tagged D3 (N-terminus) or D5 (C-terminus) truncations of KIF22 and treated with EGF (10 ng/ml) for 15 min, followed by fixation and staining for DAPI (blue), FLAG (green) and EGFR (red). EGFR staining is shown as single (white) channel images below the merged images; red asterisks denote FLAG-expressing cells. **(B)** Quantification of junctional EGFR levels after stimulation with EGF from experiments shown in (A). Data are

mean ± SEM pooled from least 40 fields of view across 2 independent experiments. **p<0.005. **(C)** Representative image of KIF22-D3 expressed in KIF22 siRNA-treated A549 cells treated with EGF for 15 min followed by fixation and staining for EGFR (red) and KIF22-D3-FLAG (green). White arrows denote areas of colocalised EGFR and KIF22-D3 at the plasma membrane. **(D)** Representative images of pEGFR staining in KIF22 siRNA-treated cells re-expressing KIF22-D3-FLAG after EGF treatment (15 mins; 10 ng/ml). Cells were fixed and stained for pEGFR (red) and FLAG (green). **(E)** Representative images of control or KIF22 siRNA-treated CAR-KD A549 cells co-expressing FLAG-tagged D3 mutants of KIF22 treated with EGF (10 ng/ml) for 15 min followed by fixation and staining for DAPI (blue), FLAG (green) and EGFR (red). Channels, asterisks as described in (A). Graph shows quantification of junctional EGFR abundance after stimulation with EGF, presented as mean ± SEM. **p<0.005. All data was analyzed for statistical differences using 2-way ANOVA. **(F)** Proposed model of KIF22 function on EGFR and CAR upon EGF binding: EGF binding to EGFR drives MAPK activation, PKCδ activation and phosphorylation of CAR. EGFR activation also promotes KIF22-CAR binding and decreases KIF22-dependent microtubule dynamics. Resulting stabilized microtubules promote EGFR retention at plasma membrane and enhances EGFR signaling.